

X International Conference on Structural Dynamics, EURODYN 2017

# An integrated approach to payload oscillations control in harbor cranes via semi-active vibration absorbers: modeling, simulations and experimental results

Andrea Arena<sup>a</sup>, Walter Lacarbonara<sup>a,\*</sup>, Arnaldo Casalotti<sup>b</sup>

<sup>a</sup>Department of Structural and Geotechnical Engineering, Sapienza University of Rome, Via Eudossiana 18, 00184 Rome, Italy

<sup>b</sup>Department of Mechanical and Industrial Engineering, University of Roma Tre, Via della Vasca Navale 81, 00146 Rome, Italy

---

## Abstract

Semi-active vibration absorbers (AVAs) are proposed to suppress large amplitude oscillations in container cranes during maneuvers and wind forcing. The AVA design and optimization are achieved via suitable nonlinear models, numerical simulations and laboratory as well as full-scale tests. A comprehensive nonlinear modelling, featuring a full three-dimensional crane model and the adaptive vibration control architecture, is devised. The container is modeled as a rigid body elastically suspended from the trolley traveling along the crane boom. Two identical AVAs are introduced by coupling the equations of motion of the control devices - which include the impact laws with rubberized (visco-elastic) end stops - with the container crane dynamics. Suitable parametric analyses are carried out to study and optimize the control devices. Full-scale experiments are performed to validate the semi-active control architecture and show its practical feasibility.

© 2017 The Authors. Published by Elsevier Ltd.

Peer-review under responsibility of the organizing committee of EURODYN 2017.

**Keywords:** Container cranes, Vibration absorbers, Semi-Active Control, Wind loads

---

## 1. Introduction

The productivity in port transshipment hubs has always been linked to the efficiency of container cranes. These are huge machines adopted for cargo movement which have to provide high precision during containers maneuvering in the lowest possible time. Moreover, the presence of strong, gusty winds in harbors can affect the cranes efficiency through a drastic increment of collisions and can further compromise the safety of workers. In most of the port transshipment hubs the performance of such machines relies on the ability of the operators to control the containers oscillations while maximizing the maneuvering speed.

Typical active control strategies adopted to mitigate unwanted payload oscillations are either based on trolley motion control or on the hoisting cable length variations [1–4]. However, active controllers tend to be switched off by the crane operators since the controllers interact with the maneuver commands dictated by them thus making the

---

\* Andrea Arena. Tel.: +39-06-44585885.

E-mail address: [andrea.arena@uniroma1.it](mailto:andrea.arena@uniroma1.it)

operators direct control more difficult. This is why passive or semi-active devices, not interfering with the operators effected commands, are here investigated. Because the frequency of the pendular motion of the container varies during the typical working maneuvers, semi-active vibration absorbers are designed to change their stiffness and damping so as to ensure maximum energy transfer.

There is a wide literature on container cranes models [5–8]. The authors of this work proposed a 3D model accounting both for the elasticity of the variable-length hoisting cables and the deformability of the crane boom [9–11]. Such full 3D model accounting for the boom elasticity highlighted the likelihood of parametric interactions between the dynamics of the boom and the container pendular motions [11]. The here employed model accounts only for the elasticity of the four hoisting cables and the 3D container rigid-body dynamics. Moreover, the finite stroke of the AVAs coupled with the container dynamics motivated the study of their impacts with rubberized stops modeled as visco-elastic barriers.

The effectiveness of the proposed control system is first investigated via parametric numerical simulations showing the better performance of the semi-active system compared to that of passive absorbers. Full-scale experiments carried out in the port of Cagliari prove the feasibility of the control architecture.

## 2. Problem formulation

The modeling approach proposed to study the effects of the control action neglects the interaction between the crane structure elasticity and the suspended container. The container motion is influenced by the hoisting cables characteristics and the container size. As shown in Fig. 1, quayside cranes are steel structures made of movable vertical frames supporting on their top a truss girder on which the trolley, driven by an operator, can travel across the boom. Moreover, the operator commands the length of the hoisting cables.

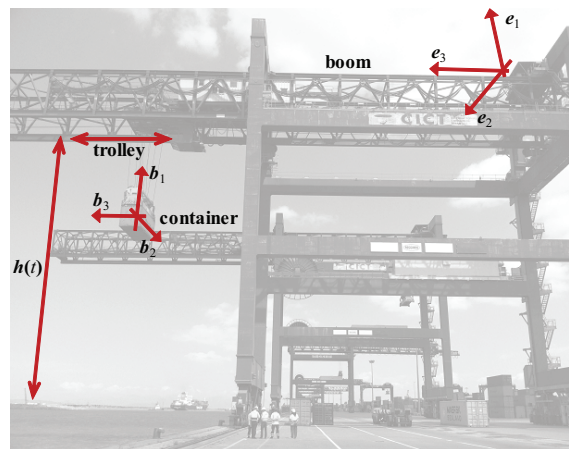


Fig. 1: The QC-7 container crane at the Cagliari International Container Terminal (CICT), Cagliari, Sardinia Italy.

By considering in Fig. 1 the fixed Cartesian frame  $(e_1, e_2, e_3)$  and two body-fixed moving frames having their origin in the center of the trolley and in the container center of mass, respectively, generalized coordinates are introduced to describe the position and rotations of the container. In consonance with [10], the current configuration of the container-crane system is described by the position vector  $p(t)$  of the container center of mass and the vector  $q(t)$  that gives the position of the trolley center of mass. The finite rotations of the container-fixed frame are parameterized by the sequences of rotation angles  $(\phi_1(t), \phi_2(t), \phi_3(t))$ . The six generalized coordinates are then listed in the vector  $\xi(t) = (p_1(t), p_2(t), p_3(t), \phi_1(t), \phi_2(t), \phi_3(t))$ .

To obtain the equations of motion governing the dynamics of the container-crane system, the Lagrangian  $L$  of the system is computed as  $L = K - V - W_c$  where  $V$  and  $K$  denote the potential and kinetic energies of the container, and  $W_c$  is the cables stored energy. Thereafter, the six equations of motion are derived according to the Euler-Lagrange

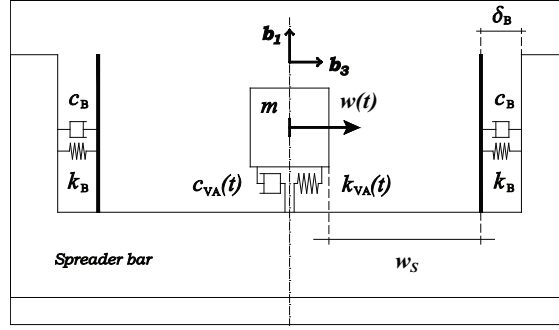


Fig. 2: Model of the AVA with the visco-elastic end stops.

equations

$$\frac{d}{dt} \left( \frac{\partial L}{\partial \dot{\xi}_k} \right) - \frac{\partial L}{\partial \xi_k} + d_k \dot{\xi}_k = F_k, \quad k = 1, \dots, 6, \quad (1)$$

where the classical damping terms proportional to the velocity of the system are taken into account through the following expressions  $d_{p_j} = 2\zeta \omega_{p_j} M$ ,  $d_{\phi_j} = 2\zeta \omega_{\phi_j} J_j^M$ ,  $j = 1, 2, 3$ , being  $\zeta$  the damping ratio,  $\omega_{p_j}$  and  $\omega_{\phi_j}$  the natural circular frequency of the  $j$ th mode,  $M$  and  $J_j^M$  the mass and the  $j$ th moment of mass of the container, respectively. The  $k$ th generalized force  $F_k(t)$  accounts for the loads generated on the container by the wind action [10], whereby the simplified modeling of the aerodynamic forces on a fixed bluff body [12] was adopted. To account for wind gust effects, the time dependence is described by the 1-COSINE time function  $G(t)$ .

### 3. Vibration absorbers equations of motion

Two VAs are placed on top of the container so that the two masses oscillate along the  $\mathbf{b}_3$  direction. By letting  $\mathbf{r}_{VA,1}$  be the relative position of the AVA centers of mass with respect to the container along direction  $\mathbf{b}_3$ , the position of the AVA masses is described by

$$\mathbf{p}_{VA}(t) = \mathbf{p}(t) + \mathbf{r}_{VA}(t) \quad \mathbf{r}_{VA}(t) = r_{VA,1} \mathbf{b}_1 + w(t) \mathbf{b}_3 \quad (2)$$

where  $w(t)$  describes the AVA motion. Thus, by letting  $m$  be the AVA mass (typically prescribed as mass ratio  $\varrho = m/M$ ), the kinetic and potential energies can be evaluated as

$$K_{VA} = \frac{1}{2} m \dot{\mathbf{p}}_{VA}(t) \cdot \dot{\mathbf{p}}_{VA}(t), \quad V_{VA} = m g \mathbf{p}_{VA}(t) \cdot \mathbf{e}_1. \quad (3)$$

Moreover, the AVA elastic stored energy reads:  $W_{VA}^E = \frac{1}{2} k_{VA}(t) w(t)^2$ .

Therefore, the overall system Lagrangian, accounting for the AVA system, becomes

$$L = K + K_{VA} - (V + V_{VA}) - (W_{VA}^E + W_c). \quad (4)$$

The AVA stroke is bound by the limits given by the available traveling space (i.e., the container width). Let  $\bar{w}_s$  be the maximum free length that the AVA mass can possibly traverse along one direction (i.e.,  $\mathbf{b}_3$  or  $-\mathbf{b}_3$ ). The stroke of the mass is fixed as a percentage of  $\bar{w}_s$ . To overcome the drawbacks of hard impacts, rubberized stops are considered via Kelvin-Voigt elements with the mechanical parameters typical of hard rubber (Young modulus  $E_B = 3.0 \cdot 10^7 \text{ N/m}^2$ ). By considering a rubber thickness equal to  $\delta_B$ , the stops can be represented by an equivalent stiffness and damping denoted by  $k_B$  and  $c_B$ , respectively (e.g., for  $\delta_B = 0.15 \text{ m}$ ,  $k_B = 4.32 \cdot 10^7 \text{ N/m}$  and  $c_B = 3502 \text{ Ns/m}$ ).

As shown in Fig. 2,  $w_s$  represents the oscillation amplitude at which the AVA mass  $m$  touches the barrier while  $\delta_B$  represents the physical width of the end stop region. Thus, when  $|w(t)| < w_s$  there is no interaction between the AVA mass and the barrier. On the contrary, when  $|w(t)| \geq w_s$ , the AVA mass collides with the right (or left) end stop which reacts delivering the viscoelastic force  $\mathbf{f}_B(t) = -F_B(t) \mathbf{b}_3$ . A further condition is superimposed to the AVA motion. If  $|w(t)| = w_s + \delta_B$ , a rigid impact occurs and is modeled by adopting Newton's law of impact with a prescribed coefficient of restitution.

The conditions regulating the free AVA motion and interactions with the end stops can be thus summarized as

$$\begin{aligned} |w(t)| &\geq w_s, \quad F_B(t) = -\{k_B [w(t) - \text{sgn}(w(t))w_s] + c_B \dot{w}(t)\}, \\ |w(t)| &< w_s, \quad F_B(t) = 0, \\ |w(t)| &= w_s + \delta_B, \quad \dot{w}(t) = -e \dot{w}(t), \end{aligned} \quad (5)$$

where  $e$  is the coefficient of restitution of steel (the lateral plates confining the absorber system) (i.e.,  $e = 0.6$ ). Finally, the equations of motion can be obtained as

$$\frac{d}{dt} \left( \frac{\partial L}{\partial \dot{\xi}_k(t)} \right) - \frac{\partial L}{\partial \xi_k(t)} + c_k \dot{\xi}_k = F_k, \quad (k = 1, \dots, 6), \quad \frac{d}{dt} \left( \frac{\partial L}{\partial \dot{w}(t)} \right) - \frac{\partial L}{\partial w(t)} + c_{VA}(t) \dot{w}(t) = F_B(t) \quad (6)$$

where  $c_{VA}(t)$  denotes the AVA damping coefficient.

**Vibration absorbers tuning.** It is common practice in the literature to express  $k_{VA}$  and  $c_{VA}$  through the optimal parameters (frequency ratio  $\alpha_{\text{opt}}$  and damping ratio  $\zeta_{\text{opt}}$ ) given as function of the mass ratio  $\rho$  (ratio between the AVA mass  $m$  and the container mass  $M$ ) according to

$$k_{VA}(t) = m \omega_{p_3}^2(t) \alpha_{\text{opt}}^2, \quad c_{VA}(t) = 2 \zeta_{\text{opt}} \sqrt{m k_{VA}(t)}. \quad (7)$$

Starting from the original formulas for the optimal parameters  $\alpha_{\text{opt}}$  and  $\zeta_{\text{opt}}$  due to Den Hartog [13], Ioi and Ikeda [14] and several other authors [13,15] proposed variants depending on the loading conditions. An overview of the most used formulas is given in Tab. 1. Since our goal is to minimize the pendular payload oscillations described by  $p_3(t)$  and caused by base motions (trolley) or wind, the expressions reported in [15] were adopted.

	Chen, Kareem [15] (autonomous excitation)	Den Hartog [13] (harmonic)	Den Hartog [13] (base excitation)
$\alpha_{\text{opt}}$	$\frac{1}{1+\rho}$	$\frac{1}{1+\rho}$	$\frac{1}{1+\rho} \sqrt{1 - \frac{\rho}{2}}$
$\zeta_{\text{opt}}$	$\sqrt{\frac{\rho}{1+\rho}}$	$\sqrt{\frac{3\rho}{8(1+\rho)}}$	$\sqrt{\frac{3\rho}{8(1+\rho)(1-\rho/2)}}$

Table 1: Optimal tuning parameters.

The analyses here performed are based on the geometrical and mechanical characteristics of the cranes operating in the port of Cagliari and provided by the CICT group. The container chosen for the numerical simulations is a 40 ft container; the damping coefficient adopted for the container-crane system was identified via full-scale experiments reported in [10]. Since the hoisting cables length  $l_i(t)$  affects the natural frequency of the container-crane system, the natural frequencies  $\omega_{p_j}$  and  $\omega_{\phi_j}$  used to define the damping coefficients  $d_{p_j}$  and  $d_{\phi_j}$ , are themselves function of the height  $h(t)$  and are determined as the solution of the eigenvalue problem associated with the equations of motion.

### 3.1. Passive control architecture

First the capability of passive vibration absorbers (VA) to damp out the container oscillations is investigated. The devices are tuned with the fundamental pendular frequency evaluated in the final target position of the container, so as to have the VAs perform best when the vertical motion is completed.

The performance of a passive control system depends sensibly on the tuning condition, but it is also largely influenced by the mass ratio  $\rho = m/M$ . The dynamical response of a 40 ton container (the maximum allowable mass) is evaluated when subject to a typical bell-shaped maneuver subject to side winds. The uncontrolled container oscillations are represented by the red solid line shown in Fig. 3, while the black, dashed black, and gray lines represent the response of the container endowed with three different absorbers with  $m = (895, 450, 225)$  kg, respectively. As expected, the best performance is achieved by the VAs with larger mass,  $m = 895$  kg (black solid line in Fig. 3).

Next, the effects of the end stops are discussed considering a bell-shaped maneuver with the 40 ton container. The end stops are modeled according to the impact laws described by Eqs. (5).

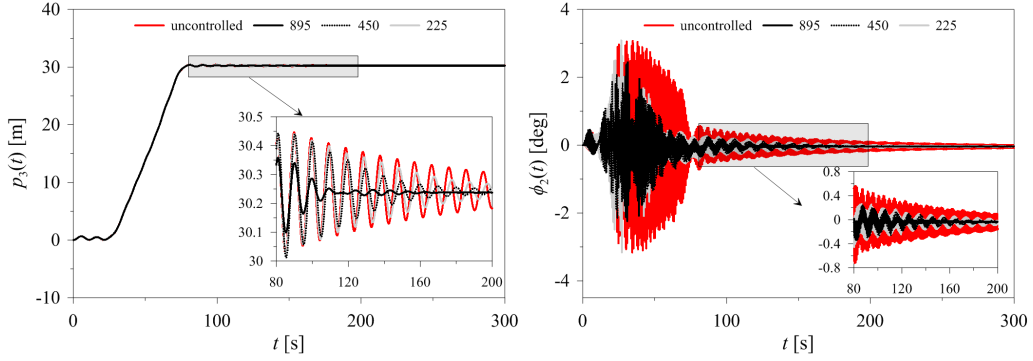


Fig. 3: Oscillations induced by a typical bell-shaped maneuver subject to side winds. The red solid lines represent the uncontrolled container motion (position and rotation). The black solid, black dashed and gray lines represent the response of the container endowed with a couple of passive linearly damped VAa with mass  $m = (895, 450, 225)$  kg, respectively. The mass of the container is  $M = 52.7$  ton.

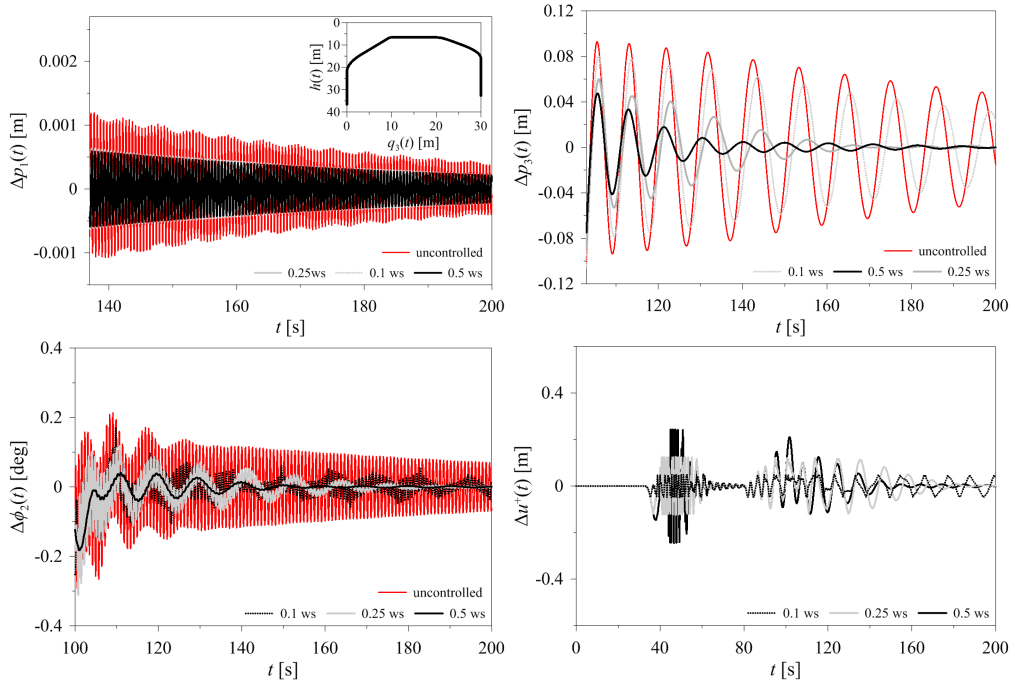


Fig. 4: Displacements and rotation induced by a typical bell-shaped maneuver. The red solid line represents the uncontrolled container motion. The gray solid, gray dashed and black solid lines represent the response of the container endowed with a couple of passive linearly damped VAs with mass  $m = 1$  ton each, while the maximum allowable stroke of the devices is  $0.1 \bar{w}_s$ ,  $0.25 \bar{w}_s$ ,  $0.5 \bar{w}_s$ . The mass of the container is  $M = 52.7$  ton.

The response of the uncontrolled system is represented by the red line in Fig. 4, while the response of the system endowed with 1 ton VAs is analyzed by adopting three values of the actuator strokes, namely,  $(0.1 \bar{w}_s, 0.25 \bar{w}_s, 0.5 \bar{w}_s)$ . As expected, when the stroke is smaller the VAs effectiveness degrades drastically since only a limited amount of energy is transferred from the container to the VAs masses.

#### 4. Semi-active control architecture

A system of semi-active VAs has the ability to tune on the fly the frequency and damping with the optimal frequency and damping that ensure the maximum energy transfer from the container to the oscillating masses. There are various

parameters that can affect the performance of a semi-active control architecture, the most important of which are the mass ratio and the speed of the frequency and damping adaptation. The sensitivity of the AVA system performance was investigated with respect to these parameters.

**Mass ratio.** The AVA parameters depend on the optimal parameters  $\alpha_{\text{opt}}$  and  $\zeta_{\text{opt}}$  which, in turn, depend on the mass ratio. Moreover, during in-service conditions  $\rho$  varies in the range  $1.9\% \div 5.6\%$  corresponding to the fully loaded case and to the empty container, respectively. The payload weight is known in real time and can thus be furnished to each AVA as an input to determine the required stiffness and damping properties. Analyses performed with different mass ratios allowed to determine the ranges of the AVA parameters.

Figure 5 shows the oscillations suffered by the lowest payload of 5 ton. The uncontrolled container is represented by the gray solid line. Two control methods are adopted. The red line represents the motion of the container when the AVA parameters are set independently from the mass ratio. On the other hand, the black line shows the container oscillation when the AVAs are tuned according also to the mass variations. Results show that the semi-active AVA varying their parameters according not only to the frequency but also to the mass ratio perform better. Yet, the control of the container oscillations given by the semi-active devices, tuned only to the actual frequency, is still significant.

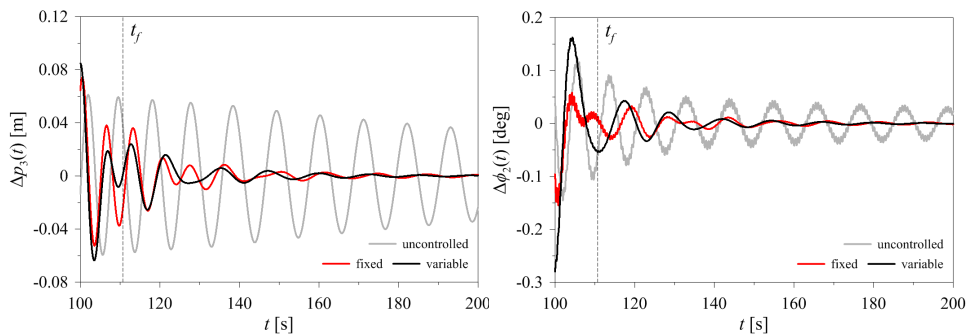


Fig. 5: Container oscillations when the container mass is equal to 5 ton ( $\rho = 5.6\%$ ). Pendular oscillations (left) and container rotations (right). The red solid lines denote the results of the system with the optimal control parameters computed according to the lower mass ratio equal to  $\rho = 1.9\%$ ; the black solid lines denote the results of the system tuned to the actual container mass.

**Speed of frequency and damping adaptation.** By considering a typical unloading maneuver from the ship to the dock (see the inset in Fig. 4), there is a phase in which the trolley travels keeping unchanged the length of the hoisting cables. At some point, the descending phase of the container is initiated towards the target position. At time  $t_{\text{TR}}$ , the trolley stops while the cable continues to be released until the container is placed on the target position at time  $t_F$ . The temporal gap ( $t_F - t_{\text{TR}}$ ) between the trolley stop and the maneuver stop is comprised in  $[0, 40]$  s depending on the speed.

This means that the semi-active AVA must reach the target frequency denoted by  $f_t$  (container frequency at the end of the maneuver) and the target damping ratio in a time shorter than  $t_F - t_{\text{TR}}$  in order to reach the optimal tuning. An example of possible frequency variations scenarios is described in Fig. 6. Starting from the baseline frequency  $f_0$  (i.e., the mean frequency value of the  $\pm 15\%$  interval allowed by the device tolerances), each AVA is supposed to reach the target frequency  $f_t$  (by changing its stiffness) according to:

- Scenario A - the AVA frequency undergoes a step-change to the target frequency  $f_t$  at time  $t_{\text{TR}}$
- Scenario B - the AVA frequency ramps up between  $t_{\text{TR}}$  and  $t_f$ , reaching the target frequency at time  $t_f$
- Scenario C - the AVA frequency ramps up between  $t_{\text{TR}}$  and  $t > t_f$ , reaching the target frequency with a certain delay
- Scenario D - the AVA frequency undergoes a step-change to the target frequency at time  $t = t_f$ .
- Scenario E - the AVA frequency ramps up between  $t_{\text{TR}}$  and  $t < t_f$  reaching the target frequency ahead of time.

Figure 7 shows the oscillations of the uncontrolled and controlled container by adopting the five frequency variations profiles shown in Fig. 6 (left part). The oscillations are induced by a maneuver which represents the worst working condition for the AVA in terms of frequency variations, since the devices are expected to cover the entire

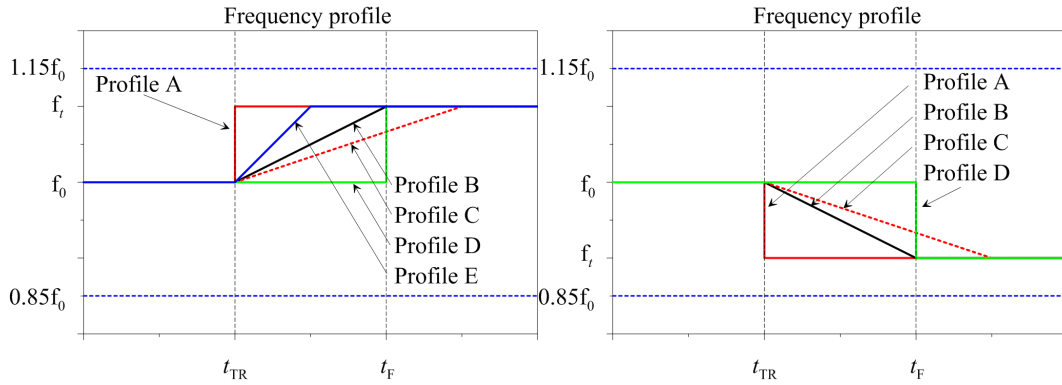
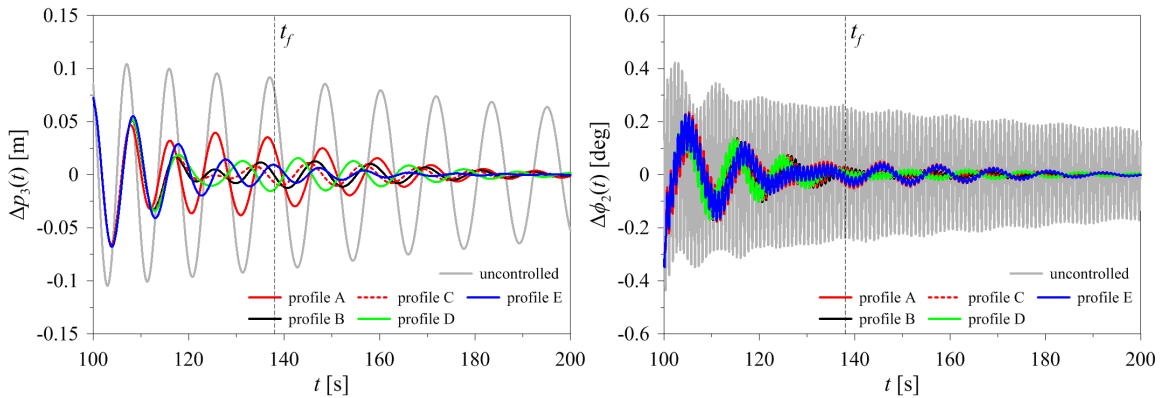


Fig. 6: Different scenarios for the AVA frequency tuning.

frequency range in the prescribed time. Scenarios A and D are to be considered as theoretical limit scenarios since step-changes in the AVA mechanical parameters are unfeasible. Scenarios C and E can represent feasible frequency profiles, although the simulations show that the slight detuning causes a loss of effectiveness of the control system. Thus, the best frequency variation profile is obtained in scenario B which thus represents the requested profile for the final design of the damping devices.

Fig. 7: Uncontrolled and controlled container crane response. The AVAs decrease their frequency in  $t_F - t_{TR} = 38$  s.

Two 1 ton AVAs were manufactured by Maurer SE (Munich, Germany) according to a design featuring a magneto-rheological actuator that effects the frequency and damping according to the control law. The devices were mounted on a Fantuzzi-Reggiane crane and various tests were performed. A sample of the acquired experimental time histories of the uncontrolled and controlled responses is reported in Fig. 8.

## 5. Conclusions

This work reported the study, optimization and validation of a semi-active control architecture for payload oscillations control in container cranes. A full 3D modeling approach had to be devised for the crane including the vibrations absorbers. For the latter the impact behavior was also considered given the presence of rubberized stops that limit the motion. To this end, visco-elastic elements were considered together with Newton's impact law for the end stops. Given the limited allowable variability of the stiffness and damping of the physical magneto-rheological device, different strategies for the frequency and damping tuning were investigated. The system was tested in full scale proving its feasibility.



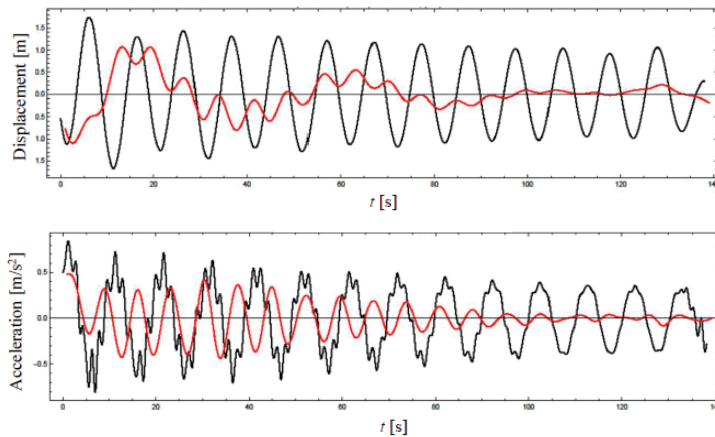


Fig. 8: Experimental time histories of displacements (top) and accelerations (bottom) of the container pendular motion: uncontrolled (black lines) vs. controlled motion (red line).

## Acknowledgements

This work was partially supported by the Sardinia State Research and Development/EU Grant CRP-49952.

## References

- [1] N. A. Nayfeh, Adaptation of Delayed Position Feedback to the Reduction of Sway of Container Cranes, Master's thesis, Virginia Polytechnic Institute and State University, 2002.
- [2] E. M. Abdel-Rahman, A. H. Nayfeh, Z. N. Masoud, Dynamics and control of cranes: A review, *Journal of Vibration and Control* 9 (2001) 863–908.
- [3] E. J. Henry, Z. N. Masoud, A. H. Nayfeh, D. T. Mook, Cargo pendulation reduction on ship-mounted cranes via boom-luff angle actuation, *Journal of Vibration and Control* 7 (1999) 1253–1264.
- [4] Z. N. Masoud, A. H. Nayfeh, Sway reduction on container cranes using delayed feedback controller, *Nonlinear Dynamics* 34 (2004) 347–358.
- [5] L. Morrish, M. P. Cartmell, A. J. Taylor, Geometry and kinematics of multi-cable lifting gear, *IMechE Journal of Mechanical Engineering Sciences, Part C* 3 (1997) 185–194.
- [6] J. B. Klaassens, G. Honderd, A. E. Azzouzi, K. C. Cheok, G. E. Smid, 3d modeling visualization for studying controls of the jumbo container crane, in: *Proceedings of the American Control Conference*, San Diego, California, 1999.
- [7] M. P. Cartmell, On the need for control of nonlinear oscillations in machine systems, *Meccanica* 38 (2003) 185–212.
- [8] M. P. Cartmell, L. Morrish, T. E. Alberts, A. J. Taylor, Controlling the nonlinear dynamics of gantry cranes, *Machine Vibration* 5 (1996) 197–210.
- [9] A. Arena, A. Casalotti, W. Lacarbonara, M. P. Cartmell, Three-dimensional modeling of container cranes, in: *Proceedings of the ASME Design Engineering Technical Conference*, 2013.
- [10] A. Arena, A. Casalotti, W. Lacarbonara, M. P. Cartmell, Dynamics of container cranes: three-dimensional modeling, full-scale experiments, and identification, *International Journal of Mechanical Sciences* 93 (2015) 8–21.
- [11] A. Arena, W. Lacarbonara, M. P. Cartmell, Nonlinear interactions in deformable container cranes, *Proc. IMechE Part C: Journal of Mechanical Engineering Science* 230 (2015) 5–20.
- [12] E. Simiu, R. H. Scanlan, *Wind effects on structures-Fundamentals and Applications to Design*, Third Edition, Wiley-Interscience Publication, 1996.
- [13] J. P. Den Hartog, *Mechanical vibration*, Dover Publications, 1985.
- [14] T. Ioi, K. Ikeda, On the dynamic vibration damped absorber of the vibration system, *The Japan Society of Mechanical Engineers* 21 (1978) 64–71.
- [15] X. Chen, A. Kareem, Efficacy of tuned mass dampers for bridge flutter control, *Journal Of Structural Engineering* (2003) 1291–1300.